Çukurova Üniversitesi
Mühendislik Fakültesi Dergisi
Çukurova University
Journal of the Faculty of Engineering
ISSN: 2757-9255 CİLT/VOLUME: 40 SAYI/ISSUE: 4 ARALIK/DECEMBER 2025

Effects Carbon Dioxide Curing on 3D Printed Cement Paste Incorporating Magnesium Oxide

Abdullah Huzeyfe AKCA [1,a], **Shiho KAWASHIMA** [2,b]

[1]*Yildiz Technical University, Department of Civil Engineering, İstanbul, Türkiye*
[2]*Columbia University, Department of Civil Engineering and Engineering Mechanics, New York, USA*

[a]***ORCID***: *0000-0003-1151-5520;* [b]***ORCID***: *0000-0002-3332-3936*

Article Info
Received : 09.05.2025
Accepted : 11.11.2025
DOI: 10.21605/cukurovaumfd.1696395

Corresponding Author
Abdullah Huzeyfe AKCA
aakca@yildiz.edu.tr

Keywords
3D printing
Carbonation
Magnesium oxide
Microstructure

How to cite: *AKCA, A.H., KAWASHIMA, S., (2025). Effects Carbon Dioxide Curing on 3D Printed Cement Paste Incorporating Magnesium Oxide. Cukurova University, Journal of the Faculty of Engineering, 40(4), 889-898.*

ABSTRACT

Magnesium oxide cement is a promising alternative to Portland Cement considering its carbon capture ability. Hydration of magnesium oxide produces magnesium hydroxide with a low compressive strength. However, after carbon dioxide curing application significant strength development can be obtained. The efficiency of carbon dioxide curing depends mainly on the depth of carbonation which is related to the surface area/volume ratio. In this study, 3D printed specimens were produced in order to enhance the rate of carbon dioxide penetration. The compression tests and microstructural investigations (TGA, SEM, XRD) were conducted on the specimens. The compressive strength of carbonated 3D printed P0M100 specimens was 7 times higher that of air cured ones. According to microstructural investigations the main form of carbonated magnesium was found to be nesquehonite.

Karbondioksit Kürünün Magnezyum Oksit İçeren 3B Baskılı Çimento Hamuru Üzerindeki Etkileri

Makale Bilgileri
Geliş : 09.05.2025
Kabul : 11.11.2025
DOI: 10.21605/cukurovaumfd.1696395

Sorumlu Yazar
Abdullah Huzeyfe AKCA
aakca@yildiz.edu.tr

Anahtar Kelimeler
3B baskı
Karbonatlaşma
Magnezyum oksit
İç yapı

Atıf şekli: *AKCA, A.H., KAWASHIMA, S., (2025). Karbondioksit Kürünün Magnezyum Oksit İçeren 3B Baskılı Çimento Hamuru Üzerindeki Etkileri. Çukurova Üniversitesi, Mühendislik Fakültesi Dergisi, 40(4), 889-898.*

ÖZ

Magnezyum oksit çimentosu, karbon yakalama kabiliyeti de düşünüldüğünde Portland Çimentosu yerine kullanılabilecek umut vadeden bir alternatif olabilir. Magnezyum oksit hidrate olduktan sonra düşük basınç dayanımına sahip magnezyum hidroksit oluşur. Ancak, karbondioksit kürleme uygulamasından sonra malzemede önemli bir dayanım gelişimi elde edilebilir. Karbondioksit kürlemenin verimliliği, esas olarak yüzey alanı/hacim oranıyla ilişkili olan karbonatlaşma derinliğine bağlıdır. Bu çalışmada, karbondioksit penetrasyon oranını artırmak için 3B yazdırılmış numuneler üretildi. Numuneler üzerinde basınç testleri ve mikro yapısal incelemeler (TGA, SEM, XRD) gerçekleştirildi. Karbonatlaştırılmış 3B yazdırılan P0M100 numunelerinin basınç dayanımı, hava ile kürlenen aynı seri numunelerinkinden 7 kat daha yüksek ölçüldü. Mikro yapısal incelemelere göre, karbonatlı magnezyumun ana formunun nesquehonite olduğu bulundu.

1. INTRODUCTION

When the high demand for concrete is taken into account, Portland cement production has an energy requirement equivalent to 7% of global energy consumption [1, 2]. In addition to carbon dioxide released during the calcination of clinker in the rotary kiln, the fuels used to heat the kiln also release carbon dioxide and the combination of these carbon dioxide emissions makes Portland cement production responsible for 8% of the global carbon emissions. [1-3]. Therefore, the increasing global concrete demand has to be met by sustainable alternatives [4-6]. These alternative products should be used instead of Portland cement or at least partially replace Portland cement in concrete mixtures [7]. Subsequently, comprehensive microstructural characterization and durability assessments are essential to evaluate the performance of these sustainable concretes.

For example, magnesium oxide cement has an important potential to become an environmentally friendly alternative to Portland cement which poses serious environmental problems in the world [8]. Especially, when magnesium oxide is derived from seawater the environmental damage during its production is minimized [9]. Additionally, magnesium hydroxide ($Mg(OH)_2$), which can be used as magnesium oxide cement source, is highly abundant in the oceans and seas [9,11-13]. Since magnesium hydroxide requires low calcination temperatures compared to Portland cement calcination the process requires considerably less amount of energy is and no toxic gases are emitted during production. Moreover, magnesium oxide powder can be carbonated to gain strength and consume carbon dioxide during concrete production, which can mean negative carbon emission [14,15]. Recent studies on magnesium based materials also showed that magnesium oxide cement has some positive effects on the properties of concrete [9,10].

On the other hand, environmental conditions during hydration and carbonation influence the products of magnesium oxide cement [16-19]. These magnesium based products are mainly nesquehonite ($MgCO_3$-$3H_2O$), hydromagnesite ($4MgCO_3$-$Mg(OH)_2$-$4H_2O$) and dypingite ($4MgCO_3$-$Mg(OH)_2$-$5H_2O$) and their strength depends mostly on the conditions during the carbonation process because carbonation causes strength development by filling the pores in the medium. For example, a few researches inferred that nesquehonite showed higher strength than other products due to its denser structure compared to other magnesium carbonate hydrate forms [20]. Unluer and Al-Tabbaa (2012) attributed this behavior to the 2.34x volume increase of magnesium hydroxide due to newly formed needle like structures in its morphology after carbonation [20]. This solid volume increase reduces the voids in the matrix and causes significant increase in rigidity and strength. However, it is very difficult to obtain high quality nesquehonite due to the effects of environmental conditions aforementioned [21]. For example, nesquehonite starts to lose its stability and may turn to other magnesium carbonate hydrates such as hydromagnesite and dypingite. Although these new forms are more stable changes in microstructure may cause reduction in material's strength [22].

Dimensions and the surface area/volume ratio of the materials are important parameters in terms of both carbon dioxide penetration and extent of carbonation. Various materials can be printed by using 3D printing technology with tailored shape and dimensions [23]. In this study it was aimed to increase the carbon penetration surface area of specimens via 3D printing techniques and specimens with infill pattern were produced by 3D printing applications [24]. In order to understand the efficiency of 3D printing application on the extent of carbonation thermal gravimetric analyses and mechanical tests were performed on the specimens.

2. EXPERIMENTAL STUDY

2.1. Materials and Mix Proportions

In the study, CEM I type 42.5 R Portland cement (PC) and reactive magnesium oxide powder (RMP) were used. The chemical compositions of the binders are given in Table 1. Acid neutralization was performed to measure the reactivity of RMP. Phenolphthalein (pH indicator) was added to the mixture of 0.28 g RMP and 50 ml 0.07 mol/l citric acid solution. In this measurement, a shorter neutralization time indicates higher reactivity. The color change, i.e. neutralization, occurred in 195 seconds.

Table 1. The chemical compositions of the binders.

	Chemical Oxide (%)							
Binder	**MgO**	**CaO**	**SiO_2**	**Fe_2O_3**	**Al_2O_3**	**Cl**	**SO_3**	**Loss on ignition**
RMP	98.2	0.8	0.35	0.15	0.1	0.35	0.05	1.7
PC	2.9	62.6	19.1	2.3	5	-	3.3	2.8

Particle size distributions of PC and RMP are given in Figure 1. 0.43 water to binder (w/b) ratio was used for 100% PC paste and 1.1 w/b ratio was used for 100% magnesium oxide paste to obtain similar yield behavior. Mixing proportions of other hybrid groups were determined considering 10% and 50% paste replacement of cement paste by volume. Binder powders and water were mixed for two minutes with a hand mixer and the paste sample was immediately poured into the syringe mold. 3D printed cylindrical specimens were produced by using four different mixtures (Table 2). Printing pattern and 3D printing of the specimens by using a syringe based 3D printer are shown in Figure 2. Two hours after printing the specimens were moved to their curing medium. The inseam for the infill pattern specimen was rotated by 3.5° for every subsequent layer. The rheological properties of mixtures affected the dimensions of the 3D printed specimens, especially their radius. The dimensions of the specimens are given in Table 3. The average radius of the 3D printed specimens was 27.3 mm ± 0.4 mm and the average height of the 3D printed specimens was 25.5 ± 0.6 mm. The wall thickness of the specimens was 4 mm. Compared to the total surface area/volume ratio of a solid cylinder, that of 3D printed specimens increased 2.5 times. By this way it is aimed to facilitate carbon dioxide penetration to the 3D printed specimens.

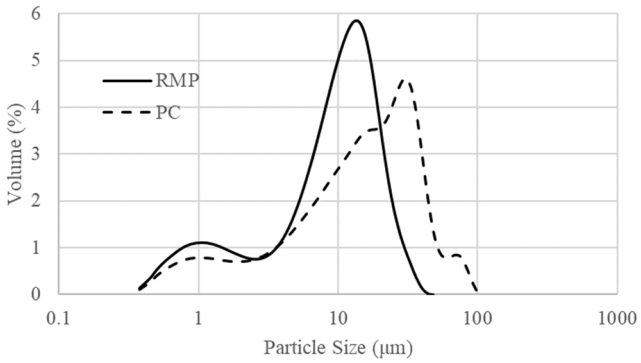

Figure 1. Particle size distributions of RMP and PC

Table 2. Mix proportions and specimen designations.

Specimen group	**w/b**	**Water (kg/m^3)**	**Portland cement (kg/m^3)**	**RMP (kg/m^3)**
P0M100	1.1	800	0	730
P50M50	0.67	690	670	360
P90M10	0.47	600	1200	70
P100M0	0.43	580	1340	0

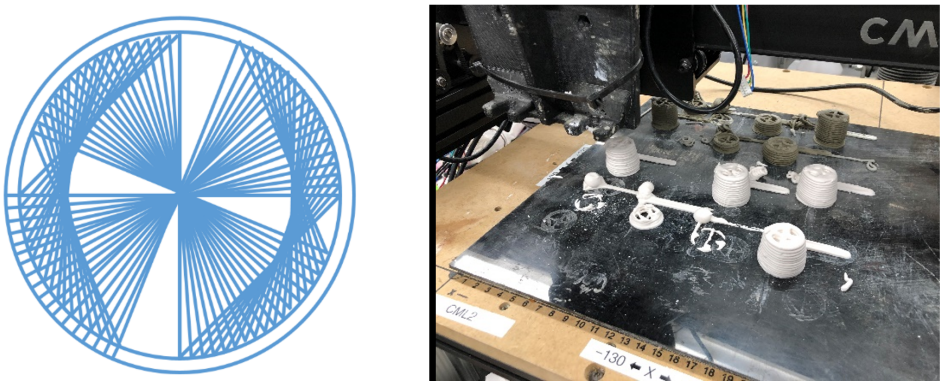

Figure 2. Printing pattern of specimens (left), 3D printing of specimens (right)

Table 3. Dimensions of the 3D printed specimens

Curing	Specimen number	P0M100 Ø (mm)	P0M100 h (mm)	P50M50 Ø (mm)	P50M50 h (mm)	P90M10 Ø (mm)	P90M10 h (mm)	P100M0 Ø (mm)	P100M0 h (mm)
%10 CO_2	1	27.3	25.1	27.1	25.2	27.8	26.2	27.6	25.4
	2	27.2	25.3	27.1	25.7	28.3	26.1	27.8	25.2
	3	27.2	25.9	27.5	25.0	27.0	26.7	26.9	25.7
Air	1	27.2	25.0	27.7	25.2	27.1	26.4	27.0	25.0
	2	27.1	25.2	27.5	25.0	27.6	26.2	27.3	25.0
	3	27.1	25.1	27.1	25.8	26.9	26.6	27.9	25.0

Ø represents the diameter of the 3D printed specimens
h represents the height of the 3D printed specimens

2.2. Rheological Tests

Binder powders and water were mixed for two minutes with a hand mixer and the paste sample was poured on a rheometer plate. Platen adjustment was completed in two minutes and each test started at 5th minute of mixing. Parallel plates were used to test the sample and the rheological properties were monitored during the test.

2.3. Curing

Specimens were subjected to CO_2 and air curing. Half of the specimens were cured in a carbon dioxide incubator at 20% ±1% CO_2 concentration, 25°C ± 2°C temperature and 85% ± 5% RH for 7 days and the remaining specimens were kept in an air curing chamber at temperature of 25°C ± 3°C and a RH of 70% ± 10% for 7 days. At the end of curing period compression tests and thermal gravimetric analyses were conducted on the 3D printed specimens.

2.4. Compression Test

Before compression tests capping was applied by using dental stone gypsum. The dimensions of the specimens varied since their rheological properties were not exactly the same. Therefore, displacement controlled loading was applied in this study instead of load-rate controlled loading. The compression tests were performed using an electromechanical testing machine (MTS Criterion C43 Universal Testing Machine, MTS, USA) with a loading rate of 0.15 mm/min as it is shown in Figure 3.

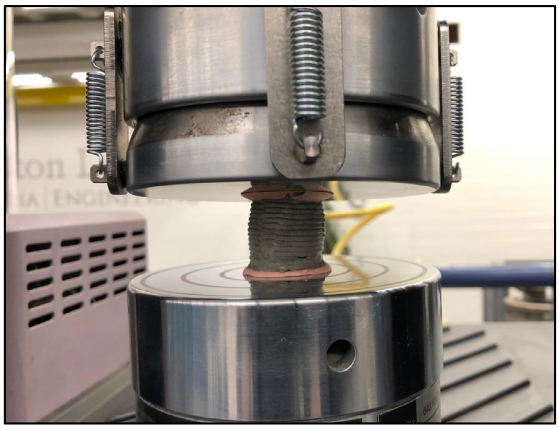

Figure 3. Compression test of a 3D printed specimen

2.5. Thermal Gravimetric Analysis

After the compression tests, the broken samples were ground into powder using a mortar and pestle and sieved using a 150 µm sieve. 20 mg of sample was taken from the powder mixture and loaded into the thermal gravimetric analyzer (TGA Q50, TA Instruments, USA). The temperature was increased linearly from 25 to 1000 °C with a heating rate of 20 °C/min under a nitrogen flow of 60 mL/min.

3. RESULTS

3.1. Rheological Test Results

Parallel plates were used to test the sample and the rheological properties were monitored during the test. Table 4 shows rheological properties of all the groups. The results showed that replacement of 10% of Portland cement paste with magnesium oxide paste had no significant effect on rheological properties of the paste but 50% replacement affected rheological properties prominently.

Table 4. Rheological properties of all the mixtures

Specimen group	Yield strength (Pa)	Storage modulus (kPa)	Plastic viscosity (Pas)
P0M100	47.6	23.84	1.21
P50M50	327.7	161.90	4.12
P90M10	62.5	48.30	1.88
P100M0	57.0	54.80	1.97

3.2. Compression Test Results

Compression tests were applied on the specimens after curing by using a uniaxial compression testing device. Cross-sectional area of each of the 3D printed specimens were determined by using Equation 1.

$$A = \frac{\pi}{4}(\emptyset^2 - (\emptyset - 2t)^2) + 2 \times (\emptyset - 2t) \times t \quad (1)$$

A is the calculated cross-sectional area, Ø is the measured diameter, t is the wall thickness (4 mm). After compression tests the peak loads were recorded and by using the calculated cross-sectional areas of the specimens their compressive strength values were calculated. The measured peak load and the calculated cross-sectional area of the specimens were given in Table 5. The average compressive strength value of each group was given in Figure 4. Also, increase in the compressive strength of specimens after carbonation was calculated and given in Table 6.

Table 5. The measured peak loads and the calculated cross-sectional areas of the specimens

		P0M100		P50M50		P90M10		P100M0	
Curing	Specimen number	P.L. (kN)	A (mm^2)	P .L. (kN)	A (mm^2)	P.L. (kN)	A (mm^2)	P.L. (kN)	A (mm^2)
%10 CO_2	1	10.10	447	11.10	443	13.12	457	8.95	453
	2	11.27	445	10.85	443	11.91	468	9.92	457
	3	9.85	445	11.53	451	11.72	441	10.15	439
Air	1	1.29	445	3.68	455	2.35	443	6.21	441
	2	1.58	443	4.35	451	3.22	453	5.71	447
	3	0.85	443	2.44	443	2.20	439	6.13	460

P.L. represents the peak load
A represents the cross-sectional area

The compressive strength of 3D printed P100M0 and P90M10 specimens was measured as 13.3 MPa and 5.9 MPa after 7 days of air curing. On the other hand, the compressive strength of 3D printed P50M50 and P0M100 specimens was measured as 7.7 MPa and 3.0 MPa after 7 days of air curing. Probably, the increased surface area of the 3D printed specimens caused rapid drying which may reduce compressive strength during air curing [23,25].

Moreover, 3D printed specimens incorporating magnesium oxide showed higher strength development after carbonation. P0M100 specimens showed 698% increase in the compressive strength while P100M0 specimens showed only 58% increase in the compressive strength after 7 days of carbon dioxide curing. According to the results it seems that carbonation of MgO has much more potential to improve the compressive strength than Portland cement. Since magnesium based specimens has much more potential for carbonation the increase surface area caused prominent strength development compared to the specimens incorporating Portland cement.

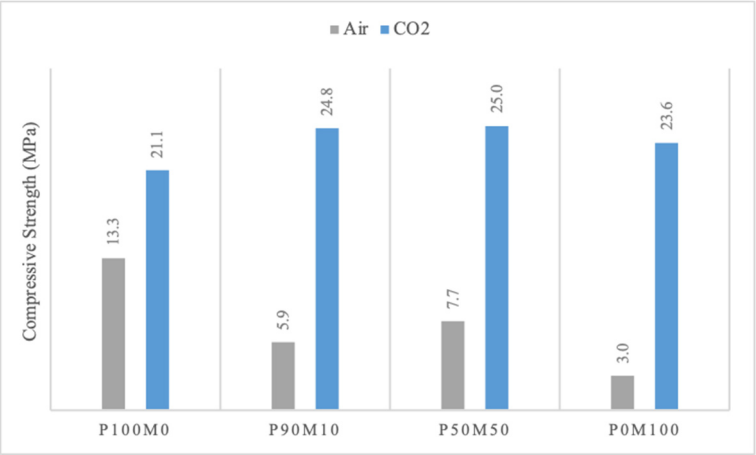

Figure 4. Compressive strength of 3D printed specimens at 7 days

Table 6. Improvement in the compressive strength of 3D printed specimens after carbonation

Specimen group	Improvement in compressive strength after carbonation (%)
P0M100	698
P50M50	223
P90M10	320
P100M0	58

3.3. Thermal Gravimetric Analysis Test Results

Powder samples were taken from the specimens after compression tests and these samples were subjected to thermal gravimetric analysis. The samples were heated up to 1000°C and after analysis Differential thermogravimetry (DTG) curves were obtained. Figure 5 shows DTG results of all the groups.

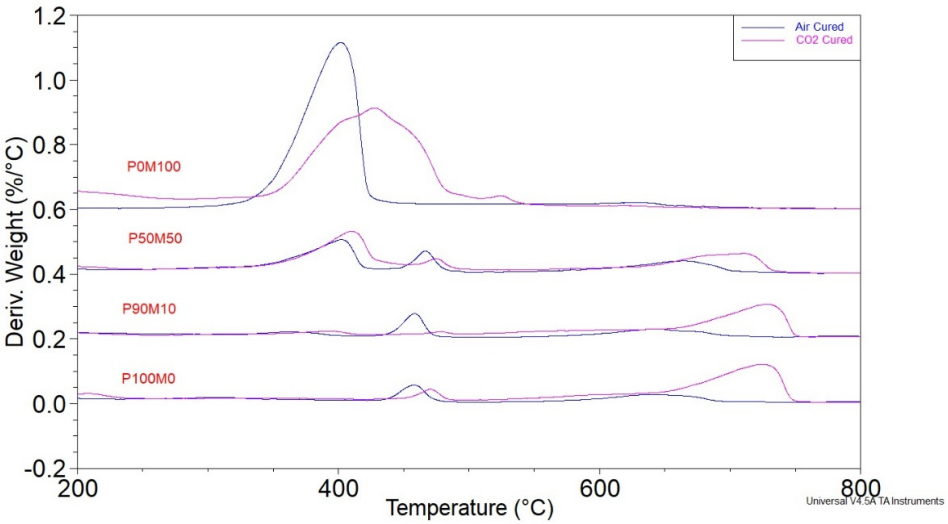

Figure 5. DTG diagrams of all the 3D printed groups

DTG peaks give information about phase changes in the material and the peaks around 450°C and 700°C in PC based materials represent dehydration of calcium hydroxide and decarbonation of calcium carbonates [26, 27]. Similarly, the peaks around 400°C and 450°C in RMP based materials represent decomposition of magnesium hydroxide and hydrated magnesium carbonates [28]. According to the results it can be concluded that carbon dioxide curing caused reduction in the amount of both hydroxide compounds in the 3D printed specimens and caused increase in the amount of both carbonated compounds. The total amount of calcium carbonate in the hybrid groups was very close to that of only PC paste after carbonation. There was an additional peak at 525 ºC representing the presence of magnesium carbonate (Magnesite) in P0M100 specimens [22].

3.4. X-ray Diffraction Test Results

X-ray diffraction (XRD) tests were conducted on the sample taken from 3D printed specimens and XRD results are given in Figure 6.

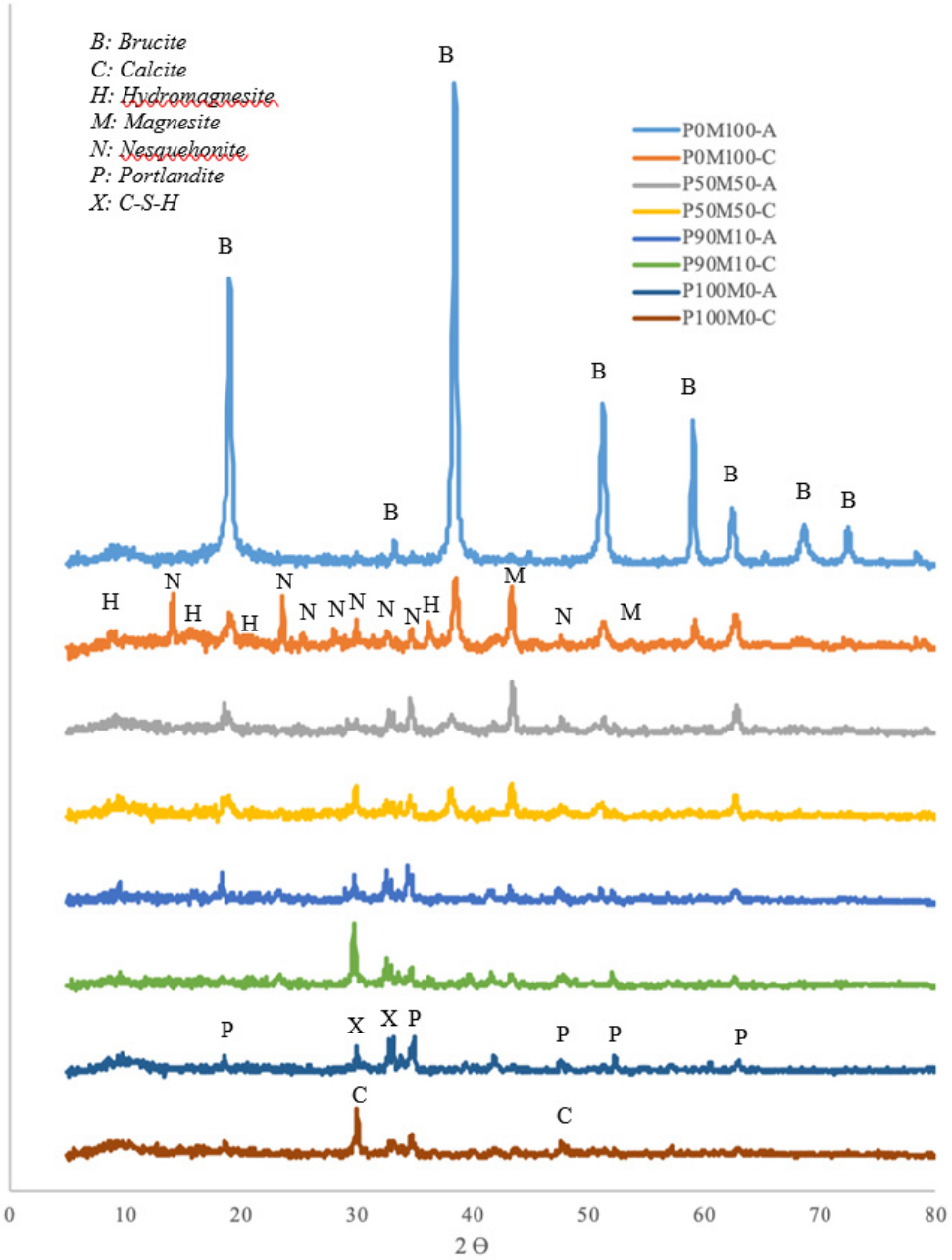

Figure 6. XRD results of 3D printed specimens

Results showed that hydroxide contents of the specimens turned to carbonated forms after carbonation. Calcium hydroxide (Portlandite) content decreased in the specimens incorporating PC and it turned to calcium carbonate (Calcite) after carbonation and similarly magnesium hydroxide (Brucite) content decreased in the specimens incorporating RMP and it turned to carbonated forms such as nesquehonite, hydromagnesite and magnesite. As it is seen in the XRD results a significant change was observed in P0M100 specimens after carbonation. Therefore, the prominent strength development in P0M100 specimens after carbon dioxide curing can be attributed to this massive phase transformation in P0M100 due to carbonation.

3.5. SEM Investigation

SEM analyses were conducted on the samples taken from 3D printed specimens and SEM images are given in Figure 7. Overall morphology of P0M100 sample after carbonation can be considered as nesquehonite while the overall morphology of P100M0 sample is calcite. There are some magnesium rich crystals, probably nesquehonite, among calcite formations in the P90M10 specimens. However, the microstructure of P50M50 is very complicated since it has various hydrated and carbonated forms in it.

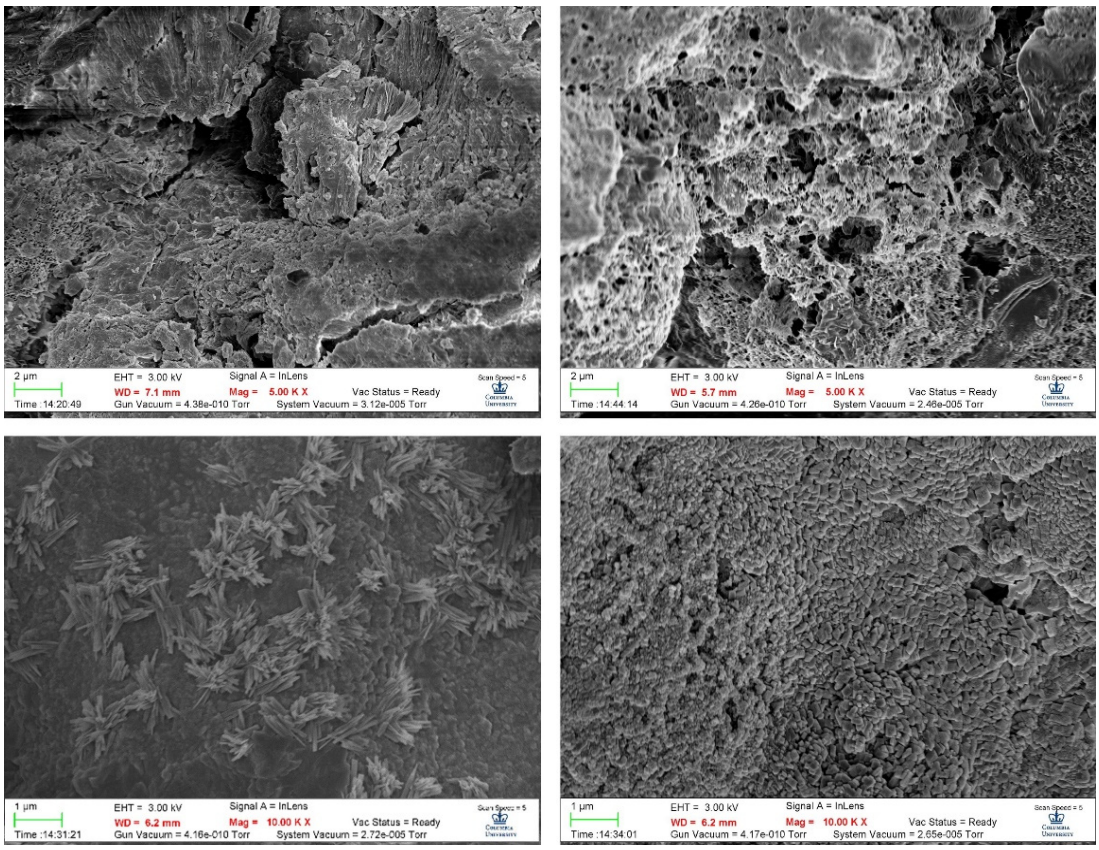

Figure 7. SEM images of P0M100 (upper left), P50M50 (upper right), P90M10 (lower left), P100M0 (lower right) after carbonation

4. CONCLUSIONS

This study investigated 3D-printed specimens produced with four mix designs (as defined in Section 2.1) and compared CO_2-cured versus air-cured conditions. For the Mg-based printable paste P0M100, CO_2 curing increased compressive strength by 7 times relative to its air-cured counterpart. The carbonated P0M100 specimens achieved strengths that were 12% higher than carbonated P100M0 and 77% higher than air-cured P100M0 controls. The strength gains are consistent with the formation of Mg-carbonate phases under CO_2 curing and the microstructural analyses identified nesquehonite as the dominant carbonate. Since nesquehonite is unstable above 50 °C [10], the thermal durability of CO_2-cured Mg-based materials may be limited and exposure to elevated temperatures can influence the carbonate content and compromise strength. Overall, CO_2 curing of Mg-based printable pastes can be considered an effective route to early and significant strength for pattern filled design.

Considering the carbon dioxide uptake capacity of magnesium based materials these results are promising for a better future. With the improvements in the technology, 3D printing applications will be more common in the world and it will be probably easier to harvest magnesium based materials from seawater [9]. Future work should target the efficiency of carbonation on larger specimens and systematic durability tests under elevated temperatures to establish service limits.

5. ACKNOWLEDGEMENTS

The authors would like to acknowledge Columbia University's School of Engineering and Applied Science (SEAS) Interdisciplinary Research Seed (SIRS) Program for financial support, and technical support by the staff of Columbia University's Carleton Laboratory. The first author is grateful for the financial support given by The Scientific and Technical Research Council of Turkey (TÜBİTAK). We also thank Siwei Ma and AlaEddin Douba for fruitful discussions throughout this work.

6. REFERENCES

1. Andrew, R.M. (2022). Global CO_2 emissions from cement production. *Earth Syst. Sci. Data, 10*, 195-217.
2. US Geological Survey (2022). *Mineral commodity summaries 2021* (Mineral Commodity Summaries, US Geological Survey, Reston, VA, USA.
3. Al-Antaki, T.S.W. & Niş, A. (2025). The influence of using basaltic pumice powder as a binder on the mechanical strength of geopolymer mortars. *Cukurova University, Journal of the Faculty of Engineering, 40*(3), 687-697.
4. Mehmetoğlu, M. (2023). Strength investigation of slag-based geopolymer composites incorporating different amounts of colemanite waste and silica fume under different exposure conditions. *Cukurova University, Journal of the Faculty of Engineering, 38*(3), 841-849.
5. International Energy Agency (2018). *Technology roadmap-Low-Carbon transition in the cement industry.*
6. Allen, M., Babiker, M., Chen, Y., de Coninck, H., Connors, S., van Diemen, R., Dube, O., Ebi, K., Engelbrecht, F., Ferrat, M., Ford, J., Forster, P., Fuss, S., Guillén Bolaños, T. Harold, J., Hoegh-Guldberg, O., Hourcade, J.C., Huppmann, D. & Zickfeld, K. (2018). Summary for policymakers, Intergovenmental Panel on Climate Change, 3-24.
7. Shi, C., Jimenez, A.F. & Palomo, A. (2011). New cements for the 21st century: The pursuit of an alternative to Portland cement. *Cement and Concrete Research, 41*(7), 750-763.
8. Ma, S., Akca, A.H., Esposito, D. & Kawashima, S. (2020). Influence of aqueous carbonate species on hydration and carbonation of reactive MgO cement. *J. CO2 Util., 41*, 101260.
9. Badjatya, P., Akca, A.H., Fraga Alvarez, D.V., Chang, B., Ma, S., Pang, X., Wang, E., Van Hinsberg, Q., Esposito, D.V. & Kawashima, S. (2022). Carbon-negative cement manufacturing from seawater-derived magnesium feedstocks. *Proc. Natl. Acad. Sci. U.S.A., 119*(34): e2114680119.
10. Akca, A.H., Ma, S., Esposito, D. & Kawashima, S. (2022). Evaluation of mechanical performance of compacted magnesium hydroxide after carbonation curing. *J. Mater. Civ. Eng., 34*(5), 1-11.
11. Moras, C.A., Cyronak, T., Bach, L.T., Joannes-Boyau, R. & Schulz, K.G. (2024). Effects of grain size and seawater salinity on magnesium hydroxide dissolution and secondary calcium carbonate precipitation kinetics: implications for ocean alkalinity enhancement. *Biogeosciences, 21*, 3463-3475.
12. Fontana, D., Forte, F., Pietrantonio, M., Pucciarmati, S. & Marcoaldi, C. (2023). Magnesium recovery from seawater desalination brines: A technical review. *Environment, Development and Sustainability, 25*(12), 13733-13754.
13. Sano, Y., Hao, Y. & Kuwahara, F. (2018). Development of an electrolysis based system to continuously recover magnesium from seawater. *Heliyon, 4*(11), e00923.
14. Haque, M.A., Dai, J.-G. & Zhao, X.-L. (2024). Magnesium cements and their carbonation curing: A state-of-the-art review. *Low-carbon Materials and Green Construction, 2*(2), 1-27.
15. Dung, N.T. & Unluer, C. (2019). Performance of reactive MgO concrete under increased CO_2 dissolution. *Cement and Concrete Research, 118*, 92-101.
16. Unluer, C. & Al-Tabbaa, A. (2013). Impact of hydrated magnesium carbonate additives on the carbonation of reactive MgO cements. *Cement and Concrete Research, 54*, 87-97.
17. Liska, M. & Al-Tabbaa, A. (2009). Ultra-green construction: reactive magnesia masonry products. *Proceedings of the Institution of Civil Engineers - Waste and Resource Management, 162*, 185-196.
18. Shand, M.A. (2006). *The chemistry and technology of magnesia.* John Wiley & Sons, New Jersey.
19. Taylor, H.F. (1997). *Cement chemistry.* Thomas Telford, London.
20. Unluer, C. & Al-Tabbaa, A. (2012). Effect of aggregate size distribution on the carbonation of reactive magnesia based porous blocks. *18th Annual International Sustainable Development Research Conference,* Hull, UK.

21. Botha, A. & Strydom, C.A. (2001) Preparation of a magnesium hydroxy carbonate from magnesium hydroxide. *Hydrometallurgy, 62*, 175-183.
22. Frost, R.L., Bahfenne, S., Graham, J. & Martens, W.N. (2008). Thermal stability of artinite, dypingite and brugnatellite-Implications for the geosequestration of greenhouse gases. *Thermochimica Acta., 475*, 39-43.
23. Zhao, H., Wang, Y., Liu, X., Wang, X., Chen, Z., Lei, Z., Zhou, Y. & Singh, A. (2024). Review on solid wastes incorporated cementitious material using 3D concrete printing technology. *Case Studies in Construction Materials, 21*, e03676.
24. Douba, A., Badjatya, P. & Kawashima, S. (2022). Enhancing carbonation and strength of MgO cement through 3D printing. *Construction and Building Materials, 328*, 126867.
25. Jung, I.D., Lee, M.S., Lee, J. & Lee, Y. (2020). Embedding sensors using selective laser melting for self-cognitive metal parts. *Additive Manufacturing, 33*, 101145.
26. Akca, A.H. & Özyurt Zihnioglu, N. (2013). High performance concrete under elevated temperatures. *Construction and Building Materials, 44*, 317-328.
27. Akca, A.H. & Özyurt, N. (2018). Effects of re-curing on microstructure of concrete after high temperature exposure. *Construction and Building Materials, 168*, 431-441.
28. Unluer, C. & Al-Tabbaa, A. (2013). Characterization of light and heavy hydrated magnesium carbonates and their thermal decomposition behavior. *Journal of Thermal Analysis and Calorimetry, 111*(3), 1973-1983.